Chin. J. Mech. Eng. (2017) 30:483–494
DOI 10.1007/s10033-017-0089-1

ORIGINAL ARTICLE

Numerical Study of Aeroacoustic Sound on Performance of Bladeless Fan

Mohammad Jafari[1] · Atta Sojoudi[2] · Parinaz Hafezisefat[3]

Received: 20 May 2016 / Revised: 8 December 2016 / Accepted: 17 January 2017 / Published online: 16 March 2017

Abstract Aeroacoustic performance of fans is essential due to their widespread application. Therefore, the original aim of this paper is to evaluate the generated noise owing to different geometric parameters. In current study, effect of five geometric parameters was investigated on well performance of a Bladeless fan. Airflow through this fan was analyzed simulating a Bladeless fan within a 2 m×2 m×4 m room. Analysis of the flow field inside the fan and evaluating its performance were obtained by solving conservations of mass and momentum equations for aerodynamic investigations and FW-H noise equations for aeroacoustic analysis. In order to design Bladeless fan Eppler 473 airfoil profile was used as the cross section of this fan. Five distinct parameters, namely height of cross section of the fan, outlet angle of the flow relative to the fan axis, thickness of airflow outlet slit, hydraulic diameter and aspect ratio for circular and quadratic cross sections were considered. Validating acoustic code results, we compared numerical solution of FW-H noise equations for NACA0012 with experimental results. FW-H model was selected to predict the noise generated by the Bladeless fan as the numerical results indicated a good agreement with experimental ones for NACA0012. To validate 3-D numerical results, the experimental results of a round jet showed good agreement with those simulation data. In order to indicate the effect of each mentioned parameter on the fan performance, SPL and OASPL diagrams were illustrated.

Keywords Bladeless fan · Computational fluid dynamic (CFD) · Aeroacoustic performance · Ffowcs Williams and Hawkings (FW-H) formulation

1 Introduction

Nowadays, the axial and radial fans are employed for various applications, such as cooling systems, air conditioning, ventilation of underground spaces, etc. The aeroacoustic performance of fans have been improved by increasing advancements in the computational fluid dynamics (CFD) and economic growth, then different types of fans with various applications and higher efficiency is offered. In 2009, a new fan was invented that its appearance and performance was different from conventional fans. The main differences of this fan with respect to conventional fans (axial and radial fans) are the multiplying intake air flow and lack of observable impeller [1]. This fan namely Bladeless/Air Multiplier fan was named on the basis of the two mentioned features. Until now, this fan is manufactured for domestic applications by diameter of 30 cm.

There are two typical fans widely used: axial and radial types, however Bladeless fans are completely distinct from those fans in mechanism aspect. Bladeless fan is similar to centrifugal fans in terms of radial impellers for intake air and also it is similar to axial fans in terms of preparing higher rate of outlet airflow. Although studies about Bladeless fan are rare in the literature, numerous experimental and numerical studies have been performed on the

✉ Mohammad Jafari
mjafari@iastate.edu

[1] Aerospace Engineering Department, Iowa State University, Ames, USA

[2] Mechanical Engineering Department, University of Tehran, Tehran, Iran

[3] Mechanical Engineering Department, Iowa State University, Ames, USA

axial and centrifugal fans. Lin, et al [2], designed a Forward–Curved (FC) centrifugal fan by numerical simulation and experimental tests. They selected NACA 0012 airfoil profile for its blade and indicated that this fan produces a higher maximum flow rate and static efficiency when the blade inlet angle is 16.5°. The influence of enlarged impeller on performance of a centrifugal fan was experimentally examined by Chunxi, et al [3]. By comparison of obtained results, they observed that flow rate, total pressure rise, shaft power and sound pressure level increased while the efficiency of fan decreased for larger blades. Govardhan, et al [4], investigated the flow field in a cross flow fan by three-dimensional simulation via the commercial software code, CFX. They simulated three impeller geometries for different radius ratio and blade angles, and then they compared their efficiency with each other. Sarraf, et al [5], experimentally studied axial fans performance for two identical fans but with different impeller thickness. They indicated that the overall performance of these two fans is same, but the fan with thicker blades contained higher rate of pressure loss by the means of 8%. Also the efficiency of the fan with thinner blades was 3% higher than the fan with thicker blade. Mohaideen [6] improved an axial fan blade by using the finite element method (FEM) and reduced 18.5% of the blade weight after optimizing on the blade thickness via stress analysis by ANSYS commercial software.

There are a lot of studies on the generated noise by various airfoils that is carried out by experimental and/or numerical approaches. Chong, et al [7], measured the generated noise by a 2-D NACA 0012 airfoil at the angles of attack 0°, 1.4° and 4.2°, in a wind tunnel. They performed their experiments for some Reynolds numbers between 1×10^5 and 6×10^5. The experimental results indicated that the pressure gradient was raised on the airfoil pressure surface by increasing of attack angle, so the noise can be produced by this phenomenon. Devenport, et al [8], carried out experimental tests on the noise propagation of NACA 0012, NACA 0015 and S831 airfoil. The obtained results indicated that the airfoils with more thickness made lower noise and revealed the different angles of attack had little influence on the sound production for NACA 0012 and NACA 0015 airfoil. Casper, et al [9], solved the equations of FW-H and developed new equations. They computed the produced noise by a NACA 0012 airfoil in a low Mach number flow. The analytical results and experimental data for NACA 0012 airfoil were in good agreement.

So far, many experimental and numerical studies have been performed on the generated sound by axial and centrifugal fans. Many researchers have used the FW-H equations to predict the sound radiation of fan by numerical simulation. Ballesteros-Tajadura, et al [10], measured the noise of a centrifugal fan via FW-H noise model using the CFD code, FLUENT. By comparing numerical and experimental noise results, they showed the FW-H model was able to predict the tonal noise with reasonable accuracy. Solving FW-H equations, Moon, et al [11] and Cho, et al [12] calculated the amount of radiated sound from an axial fan and a cross flow fan, respectively. Younsi, et al [13], used numerical simulation to predict the noise level in a HVAC forward centrifugal fan. By comparing numerical and experimental data, they showed the good agreement between simulation and the experimental data. In some papers, researchers have studied the source of generating noise in different fans by using the computational aeroacoustics (CAA) [14]. Khelladi, et al [15], calculated the noise of a high rotational speed centrifugal fan via FW-H analogy and solving the Reynolds Averaged Navier-Stokes (RANS) equations. They compared the numerical and experimental data and also evaluated the aerodynamic performance of fan. In 2009, Sorguven, et al [16], studied aerodynamic and aeroacoustic performance of two radial fans. Moreover in their study, LES turbulence modeling and FW-H noise modeling were employed. They showed a satisfied agreement of experimental and numerical results and reported FW-H model as a reasonable model for evaluating aeroacoustic performance of fans.

Although Bladeless fan is invented in 2009, but until now aeroacoustic performance of this fan has not been studied numerically or experimentally for different conditions. This fan is designed for home applications by diameter of 30 cm and the only available geometric information is mentioned in patent documentation [1]. In the present study, the effect of five geometric parameters is investigated on performance of a Bladeless fan by diameter 30 cm. The studied parameters are height of fan cross section, outlet angle of the flow relative to the fan axis, thickness of airflow outlet slit, hydraulic diameter and aspect ratio for circular and quadratic cross sections. The unsteady conservation of mass and momentum equations are solved to simulate three-dimensional incompressible flow in the Bladeless fan. The Ffowcs Williams and Hawkings (FW-H) formulation is solved to calculate the noise propagation of Bladeless fan. Firstly, the generated noise of a NACA 0012 airfoil is computed to validate aeroacoustic results by experimental data [17]. The obtained numerical results and the experimental data are in the reasonable agreement, so the FW-H model is employed to measure the tonal noise of Bladeless fan. To validate 3-D numerical simulations, the experimental results of a round jet [18] are compared with numerical simulation results. Since there is not any experimental data about Bladeless fans, round jet is selected due to much similarity. The turbulence in the Bladeless fan is simulated by standard $k - \varepsilon$ turbulence model. In order to design cross section of Bladeless fan, Eppler 473 airfoil is chosen among standard airfoils. Eppler 473 airfoil is selected because it is an appropriate airfoil for low Reynolds numbers and high similarity of this airfoil profile to original cross section (designed by inventor) [1]. The volume flow rate is calculated at a distance up to 3 times of nozzle diameter in front of the fan (around 1000 mm) [1]. The numerical results for Bladeless fan show that the investigated parameters in this study are very important to improve the fan performance. Thus these parameters should be considered to design a high performance Bladeless fan.

2 Mechanism of Bladeless Fan

This fan is produced for domestic applications and its diameter is 30 cm. The mechanism of inlet and outlet airflow from this fan is shown in Fig. 1. At the first stage, the airflow is sucked into the fan through a rotating DC brushless motor and a mixed flow impeller. The intake air is accelerated by passing through an annular aperture which the cross section of this fan is similar to an airfoil profile. Then air is pushed out from a ring shape region, so the air velocity is increased in this region. A considerable pressure difference is generated between both sides of the fan and the discharged air can be described by Bernoulli's principle. This pressure difference draws the behind and surrounding air toward front of fan. Therefore, a bladeless fan amplifies the intake air by drawing the air behind and around the fan. Thereby the inventor of this fan claims that [1] this fan multiplies intake air at about 15 times at distance 3D front of fan (around 1000-1200 mm) [1, 19]. All of described stages are shown in Fig. 1.

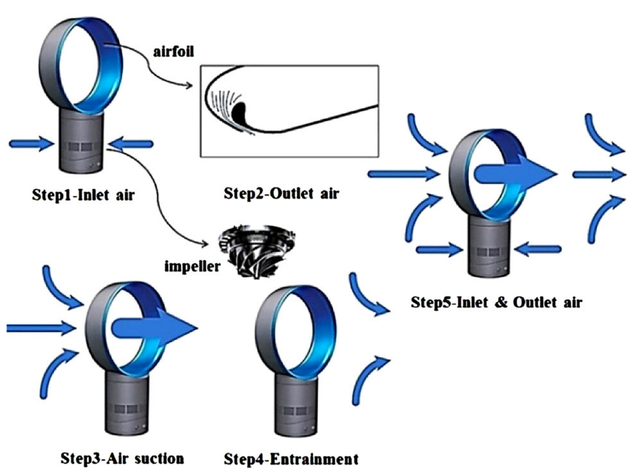

Fig. 1 Schematic of airflow motion steps from a Bladeless fan

3 Computational Method

3.1 Aerodynamic Equations

In this work, conservation equations of mass and momentum are numerically solved by to analyze unsteady incompressible flow within the Bladeless fan. The continuity equation is described by

$$\frac{\partial \rho}{\partial t} + \frac{\partial}{\partial x_i}(\rho u_i) = 0 \tag{1}$$

where i=1, 2 and 3, ρ is air density and u_i is the velocity in direction i. The momentum equations are given by

$$\frac{\partial}{\partial t}(\rho u_i) + \frac{\partial}{\partial x_i}(\rho u_i u_j) = -\frac{\partial p}{\partial x_i} + \frac{\partial \tau_{ij}}{\partial x_j} \tag{2}$$

where p is the static pressure and τ_{ij} is the stress tensor. The standard k-ε turbulence model is used to simulate turbulent flow. The standard k-ε model is a semi-empirical model that was introduced by Launder, et al [20]. The turbulence kinetic energy, k, and its rate of dissipation, ε, are described by the following equations:

$$\frac{\partial}{\partial t}(\rho k) + \frac{\partial}{\partial x_i}(\rho u_i k) = \frac{\partial}{\partial x_i}\left[\left(\mu + \frac{\mu_t}{\sigma_k}\right)\frac{\partial k}{\partial x_i}\right] + G_k - \rho\varepsilon - Y_M + S_k \tag{3}$$

$$\frac{\partial}{\partial t}(\rho \varepsilon) + \frac{\partial}{\partial x_i}(\rho u_i \varepsilon) = \frac{\partial}{\partial x_i}\left[\left(\mu + \frac{\mu_t}{\sigma_\varepsilon}\right)\frac{\partial \varepsilon}{\partial x_i}\right] + C_{1\varepsilon}\frac{\varepsilon}{k}G_k - C_{2\varepsilon}\rho\frac{\varepsilon^2}{k} + S_\varepsilon \tag{4}$$

The turbulent viscosity is also evaluated as:

$$\mu_t = C_\mu \rho \frac{k^2}{\varepsilon} \tag{5}$$

and

$$G_k = \mu_t\left(\frac{\partial u_j}{\partial x_i} + \frac{\partial u_i}{\partial x_j}\right)\frac{\partial u_j}{\partial x_i} \tag{6}$$

where G_k is production rate of turbulent kinetic energy in Eqs. (3) and (4). Y_M represents the contribution of the fluctuating dilatation in compressible turbulence to the overall dissipation rate. S_k and S_ε are user-defined source terms. In these equations, the constant parameters are $C_{1\varepsilon}$=1.44, $C_{2\varepsilon}$ =1.92, C_μ=0.09, σ_k=1.0 and σ_ε=1.3. A second order implicit scheme is used for discretization of time dependent terms in the equations. Furthermore, the second order upwind scheme has been used for convection terms and the central difference scheme for diffusion terms. The SIMPLE algorithm is applied for pressure-velocity coupling and the obtained solutions are based on time step 0.0001.

3.2 Acoustic Equations (FW-H Integral Method)

The far-field sound radiation of the turbulent flow can be extended using numerical methods. In this work, the far field noise is computed by solving the FW-H equations. The FW-H formulation [21] is the most general form of the Lighthill's acoustic analogy and it is appropriate for numerical computing of the acoustic field. This formulation is derived directly from the conservation of mass and momentum equations and employing the Heaviside function $H(f)$.The FW-H equations are written as follows:

$$\frac{1}{a_o^2}\frac{\partial^2 p'}{\partial t^2} - \nabla^2 p' = \frac{\partial}{\partial t}\{[\rho_o u_n + \rho(u_n - v_n)]\delta(f)\} - \frac{\partial}{\partial x_i}\left\{\left[p_{ij}n_j + \rho u_i(u_n - v_n)\right]\delta(f)\right\} + \frac{\partial^2}{\partial x_i \partial x_j}\left(T_{ij}H(f)\right) \quad (7)$$

in which, v_i and v_n are the surface velocity in the x_i direction and normal to the surface. u_i and u_n are the fluid velocity components in the x_i direction and normal to the surface. $H(f)$ is the Heaviside function, $\delta(f)$ is the Dirac delta function and p' is the sound pressure at the far-field location. The first and second terms on the right-hand side of Eq. (7) are monopole (thickness) and dipole (loading) surface source terms, respectively. The monopole source term is the noise produced via volume of the fluid displacement by moving walls. The loading or dipole source term is the influence of unsteady motion of the force distribution on the surface of rigid body. The third source term in the Eq. (7) is a quadrupole source term that occurs due to the flow structure. In the Eq. (7), the compressive stress tensor, p_{ij}, and the Lighthill's stress tensor, T_{ij}, are defined as follows:

$$p_{ij} = p\delta_{ij} - \mu\left[\frac{\partial u_i}{\partial x_j} + \frac{\partial u_j}{\partial x_i} - \frac{2}{3}\frac{\partial u_k}{\partial x_k}\delta_{ij}\right] \quad (8)$$

and

$$T_{ij} = \rho u_i u_j - p_{ij} + a_o^2(\rho - \rho_0)\delta_{ij} \quad (9)$$

The free-stream quantities in the mentioned equations are specified by the subscript *0*. Eq. (7) is solved by using the free-space Green function $(\delta(g)/4\pi r)$ which the complete set of solution consists of surface integrals and volume integrals. The contribution of the volume integrals becomes small when the flow is low subsonic, thus in this study, the volume integrals are dropped. Finally:

$$p'(\vec{x}, t) = p'_T(\vec{x}, t) + p'_L(\vec{x}, t) \quad (10)$$

The two terms on the right-hand side of Eq. (11), p'_T, p'_L are the thickness and loading terms, respectively that are given by

$$4\pi p_T(\vec{x}, t) = \int_{f=0}\left[\frac{\rho_o(\dot{U}_n + U_{\dot{n}})}{r(1 - M_r)^2}\right] dS + \int_{f=0}\left[\frac{\rho_o U_n(r M_r + a_o(M_r - M^2))}{r^2(1 - M_r)^3}\right] dS,$$

$$4\pi p'_L(\vec{x}, t) = \frac{1}{a_o}\int_{f=0}\left[\frac{\dot{L}_r}{r(1 - M_r)^2}\right] dS + \int_{f=0}\left[\frac{L_r - L_M}{r^2(1 - M_r)^2}\right] dS + \frac{1}{a_o}\int_{f=0}\left[\frac{L_r\{r\dot{M}_r + a_o(M_r - M^2)\}}{r^2(1 - M_r)^3}\right] dS, \quad (11)$$

where $\tau = t - r/a_0$ and

$$U_i = v_i + \frac{\rho}{\rho_o}(u_i - v_i) \quad (12)$$

$$L_i = p_{ij}n_j + \rho u_i(u_n - v_n) \quad (13)$$

The various subscripted in the Eq. (11) are the inner products of a vector or a unit vector. For example:

$$L_r = \vec{L} \cdot \vec{r} = L_i r_i \quad (14)$$

$$U_n = \vec{U} \cdot \vec{n} = U_i n_i \quad (15)$$

where $\overrightarrow{n_r}$ and $\vec{r}$ indicate outward vector to the wall and the radiation directions, respectively. Also the dot over a variable indicates a time derivative of that variable. The presented formulation is based on Farassat's [22] formulation to solve the FW-H equations.

4 Boundary Conditions

Fig. 2(a) illustrates the location of Bladeless fan within a room, 4 m in length, 2 m in width and 2 m in height. As shown in this figure, air is entered through cylindrical inlet of 9 cm diameter, beneath the annular part of the fan. Then the intake air passes to narrow gap through the annular part of the fan where the cross section is Eppler 473 airfoil profile. Simulating the below fan and its impellers is negligible due to the considerable importance of regarding top part for multiplying the amount of air leaving the Bladeless fan. Though blades have not been simulated, the boundary conditions are considered for entry in the fan blades. No slip condition is assigned to the room floor and Bladeless side wall (Blue colored parts in Fig. 2(a)) and free boundary by zero relative pressure was assigned to other walls of room. Sound receiver was considered 1m after the Bladeless fan to measure the sound emitted from the Bladeless fan. Fig. 2(b) shows the schematic of the receiver position.

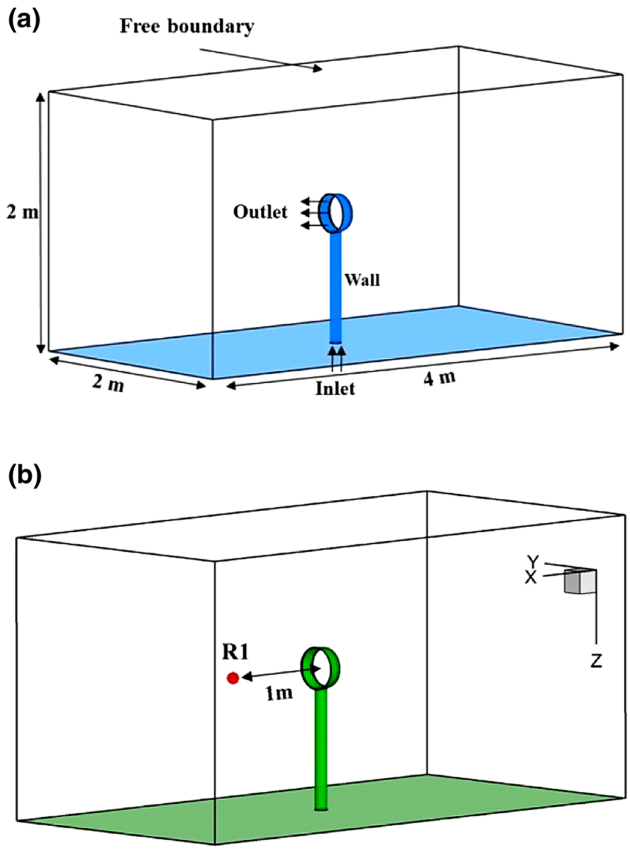

Fig. 2 (a) 3-D schematic of Bladeless fan within the computational domain, and (b) location of sound receiver

5 Geometry Investigation Parameters

Effect of five distinct geometric parameters on performance of a Bladeless fan is investigated in the present study. The first parameter is the height of fan cross section. Fig. 3(a) shows different sizes of cross sections and their dimensions in cm. 1.5 cm, 2 cm, 3 cm and 4 cm height cross sections are used to see the effect of related parameters. Airfoil length and thickness of exiting region are constant for all case studies (See Fig. 3a)) to keep the height of fan cross section as the only varying parameter.

The second investigating parameter is outlet angle of the flow relative to the fan axis. As shown in Fig. 3b), outlet angles are assigned to be 10°, 13°, 16° and 20°. Also the lengths of other airfoils are kept constant to have solo varying parameter of the outlet angle. Thickness of airflow outlet slit is 1 mm.

Thickness of airflow outlet slit is third studied parameter effecting on the Bladeless fan performance. As illustrated in Fig. 3c), three outlet slits of 1 mm, 2 mm and 3 mm are considered with for the constant amounts of airfoil length, height of cross section and outlet angle of flow (16°). Three hydraulic diameters of 30 cm, 60 cm and 120 cm are considered for investigating the effect of

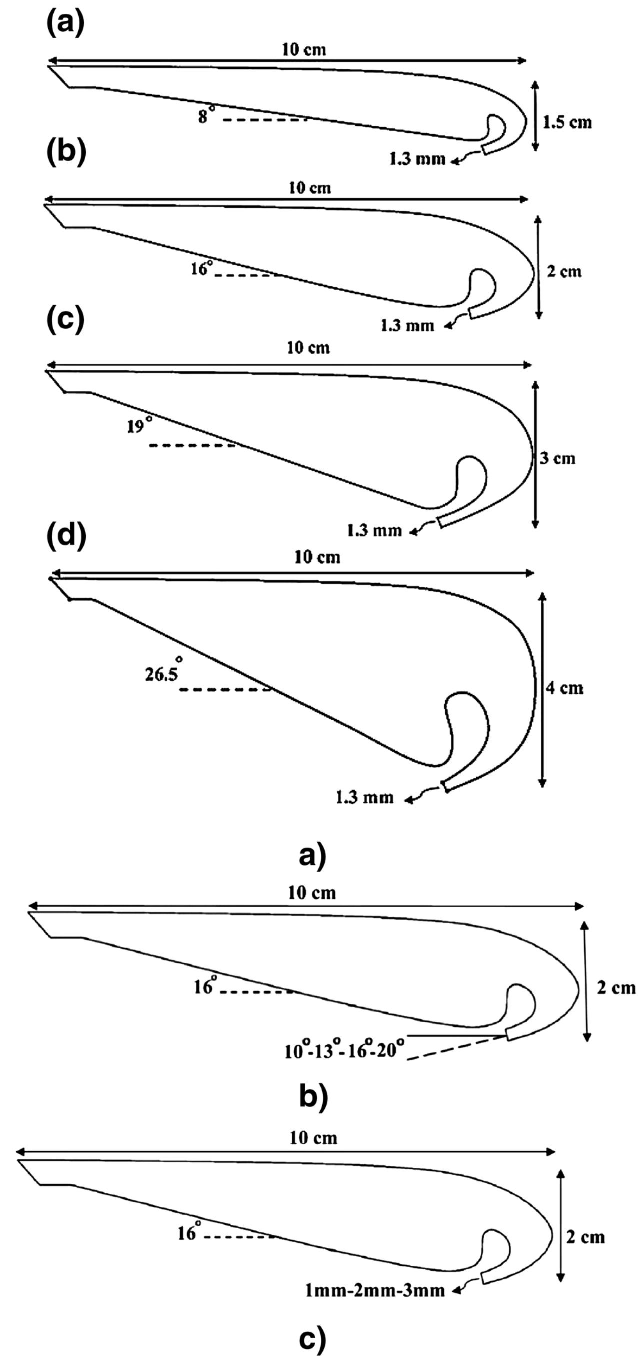

Fig. 3 a) Four distinct heights of cross sections: (a)1.5 cm, (b) 2 cm, (c) 3 cm, (d) 4 cm; b) Airfoil cross section for outlet angles of 10°, 13°, 16° and 20°; c) Airfoil cross section for three outlet slits of 1 mm, 2 mm and 3 mm

hydraulic diameter size on Bladeless fan performance (See Fig. 4(a)). Air outlet slit is 4 mm constant for the mentioned case study. Influence of aspect ratio for circular and square cross sections on performance of Bladeless fan is the last studying parameter. Fans with aspect ratios of 1, 1.5 and 2 with outlet slit of 1.3 mm are considered. Not only aspect ratio value is investigated in

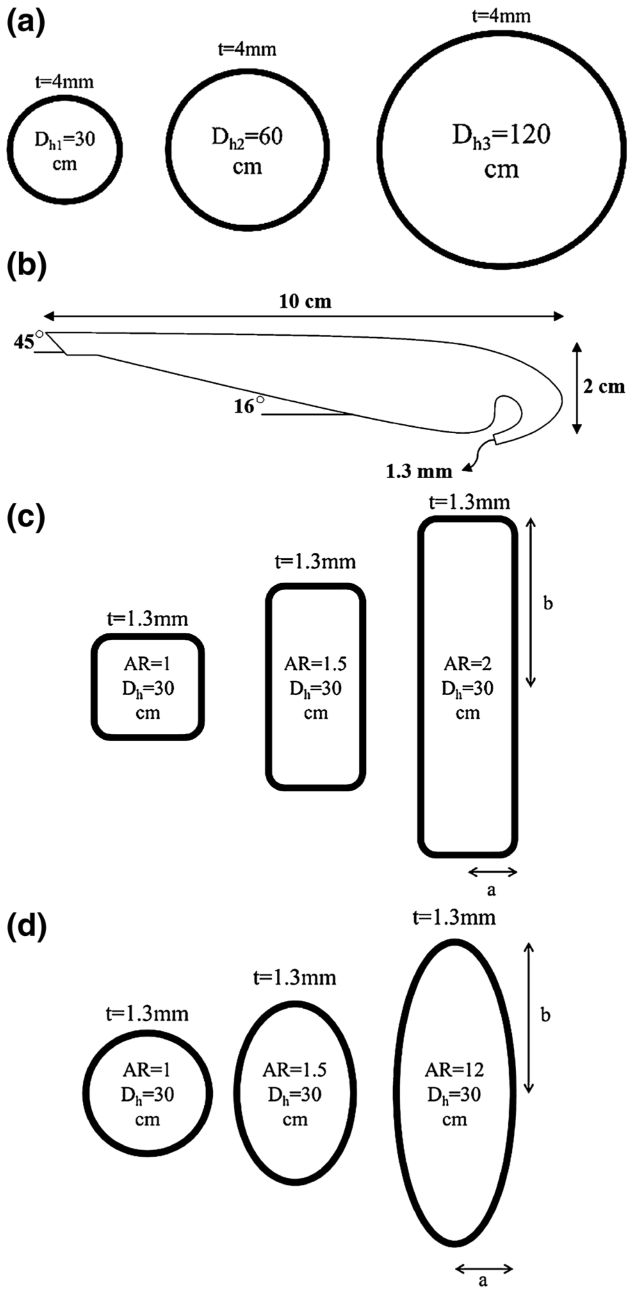

Fig. 4 (a) Schematic of airflow outlet area for three hydraulic diameters of 30 cm, 60 cm and 120 cm; (b) Studied airfoil for aspect ratio studying cases; (c) Square outlet of fan with constant hydraulic diameter of 30 cm and outlet slit of 1.3 mm; (d) Circular outlet of fan with constant hydraulic diameter of 30 cm and outlet slit of 1.3 mm

this part, but also effect of fan shape (circular or square) is studied. Characteristics of airfoil for the studied parameter in the mentioned cases are illustrated in Fig. 4(b). Outlet circular and square fan are schematically shown in Figs. 4(c) and 4(d). Value of hydraulic diameter is kept constant for these case studies to see the effect of aspect ratio on fan performance.

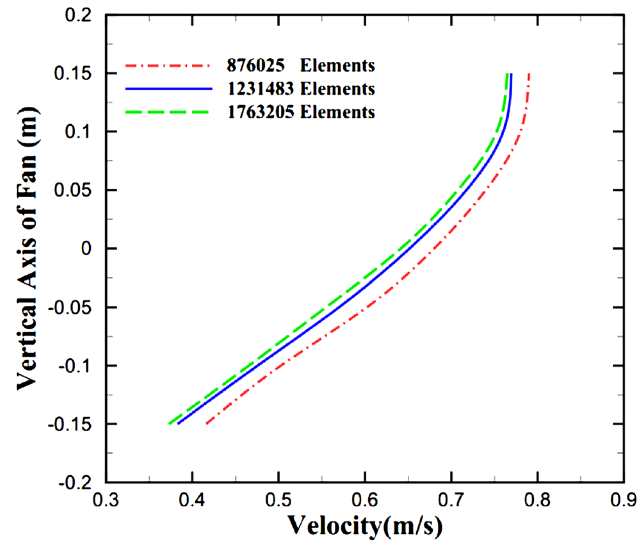

Fig. 5 Velocity profiles at a distance of 50 cm in front of the fan with inlet flow rate of 30 L/s

6 Grid Resolution

Grid independency of the simulation is carried out before simulating case studies according to cells attributed to the fan and the cub to reach a reasonable cell number. Hence, three mesh sizes with 876025, 1231483, and 1763205 cells for simulation of the fan with a diameter of 30 cm and a thickness of 1 mm outlet, has been used. As shown in Fig. 5, the velocity profiles of the exhaust air for 50 cm in front of fan are compared for the three mesh sizes. The results showed that the cell number 1231483 for the current simulation is suitable, so the number of grid cells for subsequent partitions are used. It should be noticed that for fans with a diameter larger than 30 cm the chamber is larger, so in order to increase the accuracy of the results, the more cells are used.

7 Validation

7.1 Noise Validation of NACA 0012

Simulating the two-dimensional airfoil NACA 0012, the equations of momentum and mass conservation with FW-H noise equation are used to evaluate the generated noise. In Fig. 6 the boundary conditions, and the grid size of different parts of the simulation, is shown. It is evident in this figure that the walls around the airfoil are considered 10 times the chord length of the airfoil for neglecting the effect of surrounding walls on the flow field around the airfoil [23]. Placing a noise receiver at a distance of 1.25 m from the airfoil trailing edge, the generated noise is measured. In Fig. 7 the SPL diagram for NACA 0012 airfoil at Reynolds

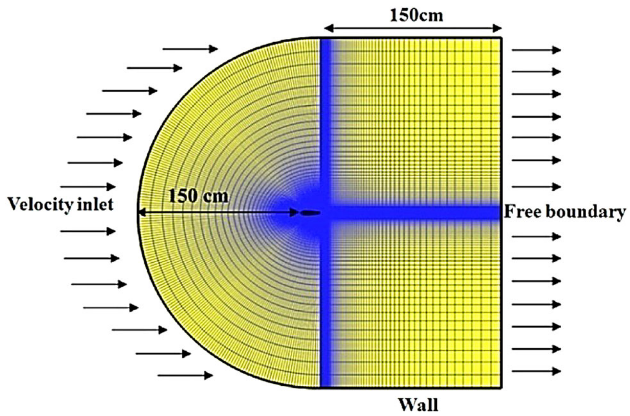

Fig. 6 Modeling, boundary conditions and cells in 2-D NACA 0012 airfoil

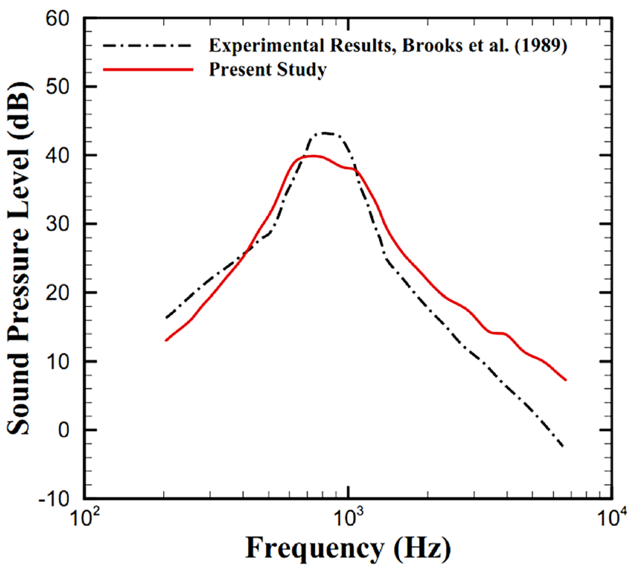

Fig. 7 Comparison of numerical results and experimental data of emitted noise for NACA 0012 airfoil at $Re=2\times10^5$

number 2×10^5, is obtained. Also the FFT algorithm is used to obtain the SPL charts. In Fig. 7, the numerical results with experimental data of Brooks, et al [17], are compared together. The comparison of the results shows that the numerical results of the produced noise value are in good agreement with experimental data for different frequencies, except for the 1000 Hz frequency range around, where the maximum sound level and the biggest difference appear. The obtained numerical results truly predict the experimental data growth or descend. Thus the FW-H equation is used to calculate the produced noise of Bladeless fan.

7.2 Validation of 3-D Fan Simulation

There is no sufficient and detailed experimental data of Bladeless fan in the literature for validation. Bladeless fan

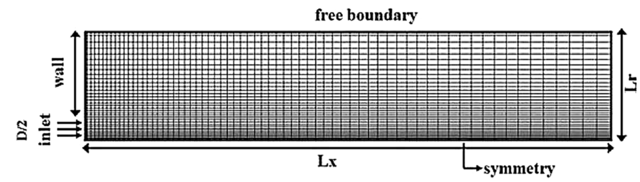

Fig. 8 Mesh and schematic of considered geometry and boundary conditions

in the exit part acts as a jet flow, so physics of both phenomena can be accounted about the same. Hence, experimental data of a circular jet [18] was used to validate Bladeless fan simulation in this study. The mesh grid and boundary conditions have been shown in Fig. 8. In order to reduce numerical costs, the jet was modeled in two-dimensional and axisymmetric. The domain dimensions were included 100 times of the jet diameter in length (Lx) and 20 times of it in width (Lr). The $k-\varepsilon$ standard turbulence model was used for turbulence modeling. The inlet velocity was set to 60 m/s uniformly and Reynolds number was 1.84×10^5.

As it can be seen in Fig. 9(a), stream wise velocity along centerline of the jet decreases. $u_{\mathrm{in,cl}}$ represents the inlet velocity and u_{cl} is the streamwise velocity at centerline of the jet. Also in Fig. 9(b), $r_{1/2}$ is jet half width that is defined as the radial distance from the centerline which the streamwise velocity equals to half of the centerline velocity at the same section. Comparison between numerical and experimental results in both above figures shows good agreement, therefore, k-ε model can simulate exit flow field of a circular jet with an acceptable accuracy.

8 Results and Discussion

8.1 Aeroacoustic Results

In general, the all fans are often used in the places where human resides are existent, so checking the amount of generated noise by the various fans is compulsory to reduce the noise level. According to the available standards, human presence in the environment, where the noise level produced by more than 80 dB, is not recommended for a long time; because it endangers the health of human hearing [24]. In this work, the effect of five geometrical parameters on the generated noise was investigated due to the importance of produced noise by this fan. In this section, the SPL charts in each section are calculated using Eq. (16) and FFT algorithm:

$$SPL = 10\log(p/p_{ref})^2 \qquad (16)$$

In the above equation p_{ref} is 20 µPa. In order to have better insight, the emitted noise level of OASPL graphs were

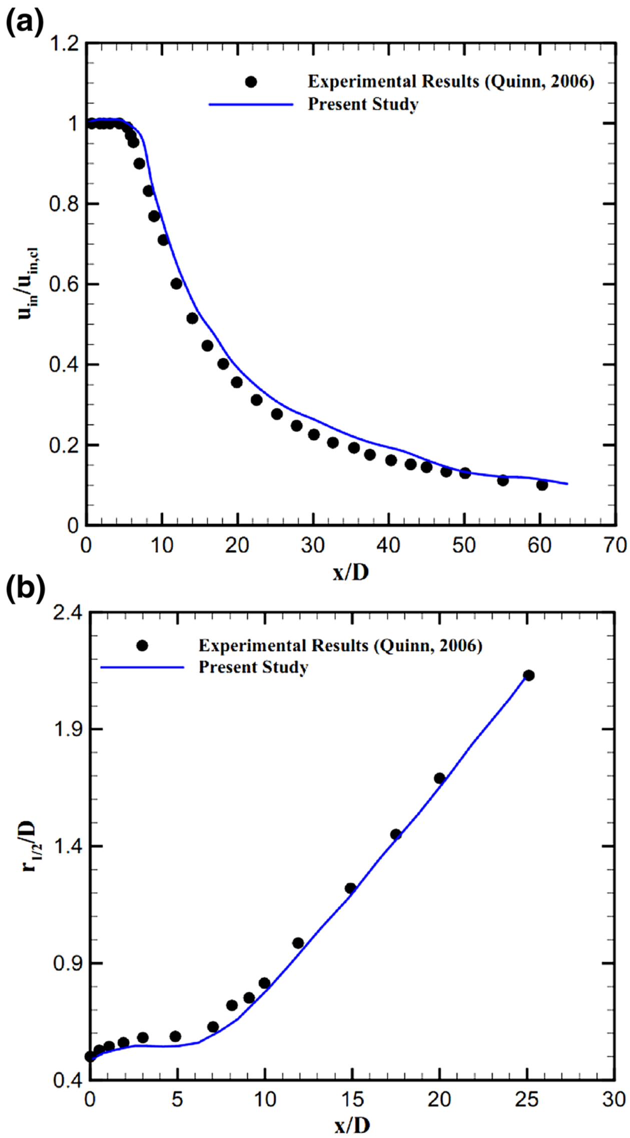

Fig. 9 (a) Streamwise velocity decay along the jet centerline; (b) Comparison between experimental and numerical results of spreading of jet

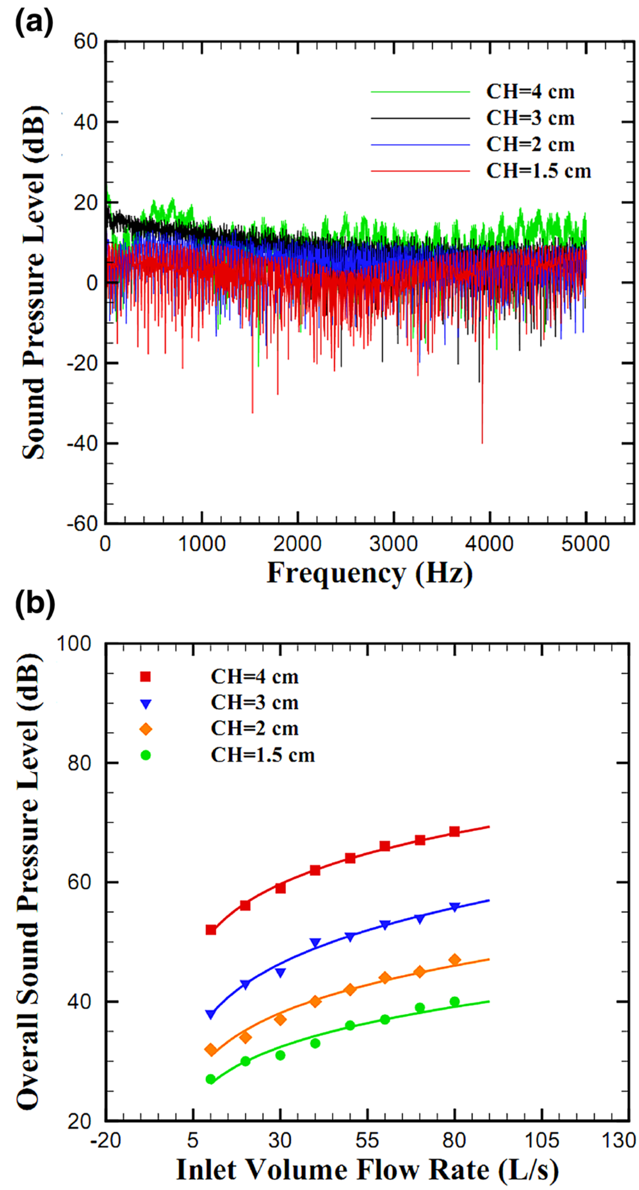

Fig. 10 (a) Sound pressure level for Bladeless fan heights of 1.5, 2, 3 and 4cm; (b) Overall sound pressure level for Bladeless fan heights of 1.5, 2, 3 and 4 cm

plotted in addition to the SPL diagrams. In Fig. 10(a), the SPL diagram is shown for different cross sections with inlet volumetric flow rate of 30 L/s. The OASPL diagram in Fig. 10(b) is plotted for cross sections of 1.5, 2, 3 and 4 cm which these curves (OASPL) are approximated by the equation ax^b. The comparison of results in Fig. 9(a) shows that the generated noise increases by growth of the amount of height fan cross section. The obtained results in this section agree well with the results of Devenport, et al [8] about the produced noise by airfoils for various thicknesses.

Fig. 11(a) indicates that the emitted noise spectrum by the Bladeless fan for different outlet angles and inlet flow rate of 30 L/s. It is clear from this figure, for low angles (10°) and high angles (20°) the fluctuations of different frequencies are higher than outlet angles 13° and 16°. In Fig. 11(b), the SPL diagram is shown for outlet angles of 10°, 13°, 16° and 20°. The comparison of the acoustic results indicates by increasing of outlet angle, the noise level increases for a constant inlet flow rate. So the design of outlet angle requires considering the effects of these parameters on the aerodynamic and aeroacoustic performance, although the effect of this parameter is less than the other parameters.

In Fig. 12(a), the generated noise spectrum is compared for different outlet thicknesses of 1, 2 and 3 mm. Also the OASPL diagram in Fig. 12(b) is plotted for different outlet thicknesses. It is obvious in this figure, the amount of

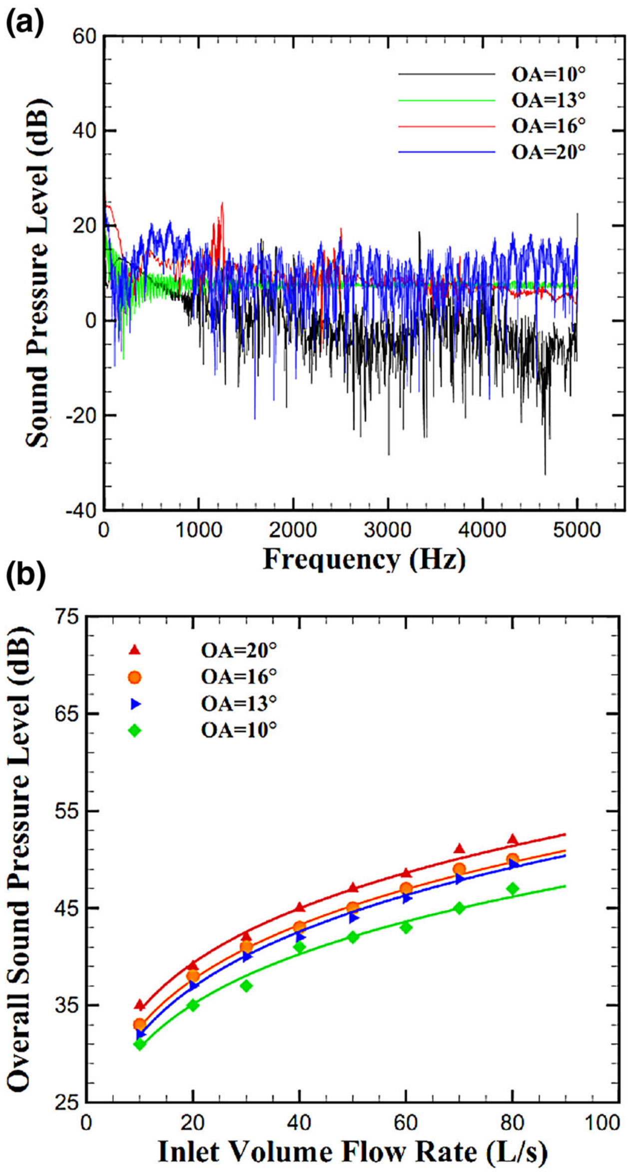

Fig. 11 (a) Sound pressure level of Bladeless fan for outlet angles of 10°, 13°, 16° and 20°; (b) Overall sound pressure level for outlet angles of 10°, 13°, 16° and 20°

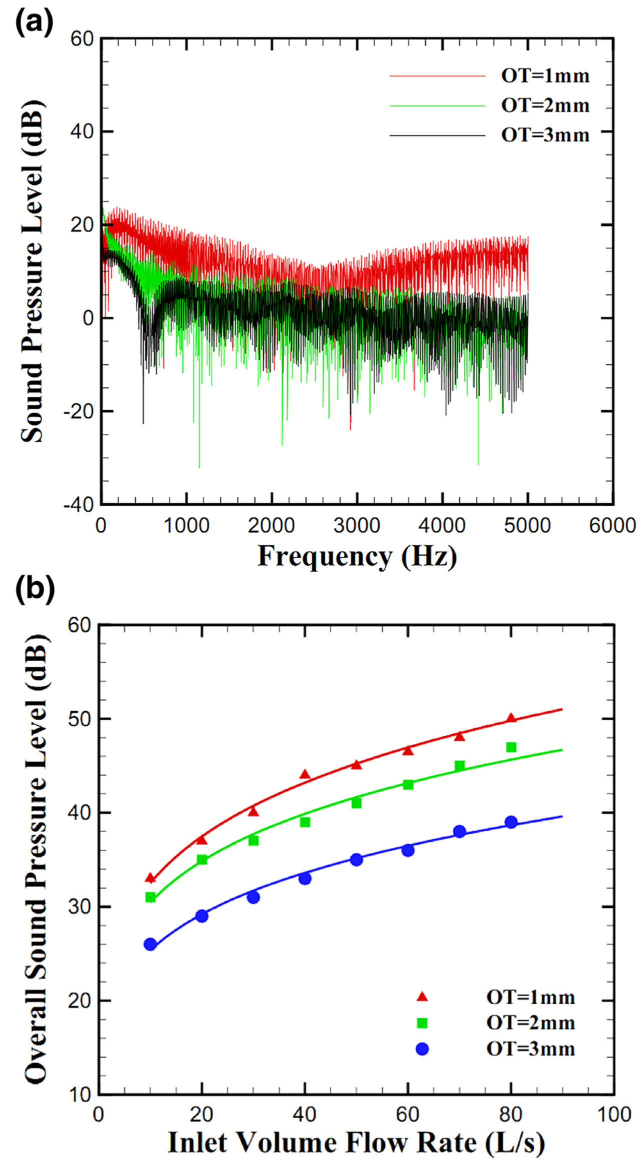

Fig. 12 (a) Sound pressure level for outlet thicknesses of 1, 2 and 3 cm; (b) Overall sound pressure level for outlet thicknesses of 1, 2 and 3 cm

emitted noise according to the law of mass conservation, the amount of outlet velocity magnitude from fan increases while the outlet thickness decreases, so the pressure fluctuations, which are the factors of noise generation, increase because of this physical phenomenon. The fourth studied parameter is hydraulic diameter of Bladeless fan. In Fig. 13(a), the SPL charts are compared for hydraulic diameters of 30, 60 and 120 cm with inlet flow rate 80 L/s. This figure shows that for a constant inlet flow rate while the fan diameter increases the sound fluctuations increase, but the generated noise decreases. The OASPL diagram is shown in Fig. 13(b) for various hydraulic diameters. It is obvious in this figure that the noise level for a constant inlet flow rate reduces while the fan diameter increases. For a constant inlet flow rate, the exhausted airflow from a small fan is more turbulent than a large fan, so the acoustic field in front of a small fan is stronger than a large one on account of more pressure fluctuations. In this paper, the last investigated parameter is the effect of aspect ratio of a circle and square fan on the emitted noise by a Bladeless fan. Therefore, the SPL and OASPL diagrams are calculated for circle and square fans. In Fig. 14(a), the SPL diagram for aspect ratios of 1, 1.5 and 2 is plotted for inlet flow rate 30 L/s. As shown in this figure, the sound fluctuations for aspect ratio 1 are higher than aspect ratios 1.5 and 2 for different frequencies.

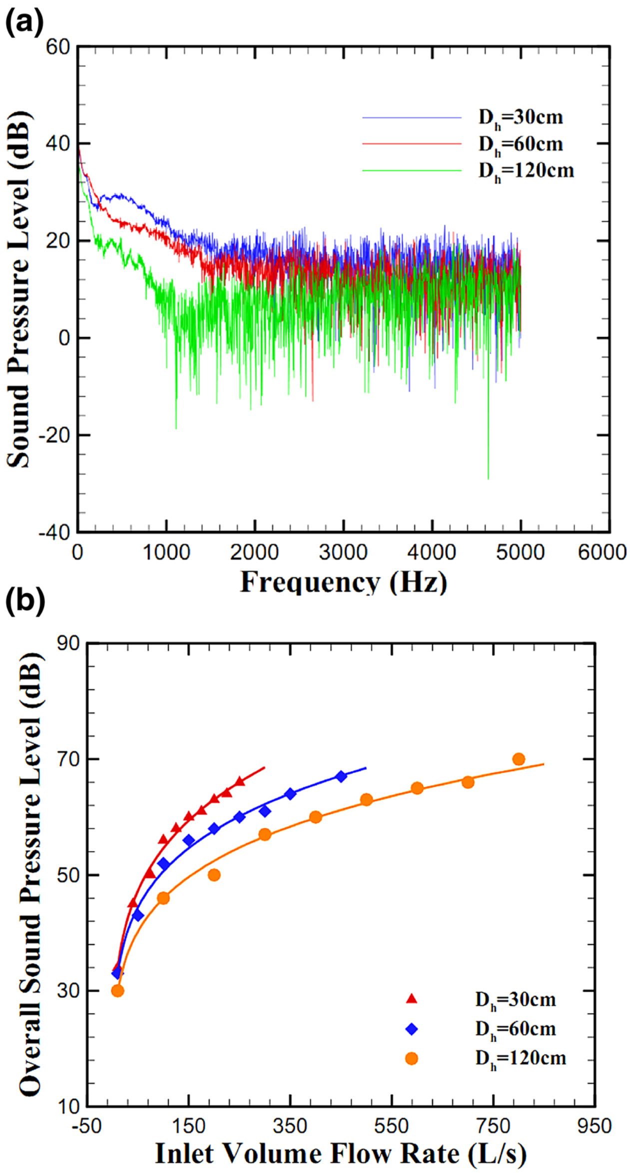

Fig. 13 (a) Sound pressure level of Bladeless fan for hydraulic diameters of 30, 60 and 120 cm; (b) Overall sound pressure level for hydraulic diameters of 30, 60 and 120 cm

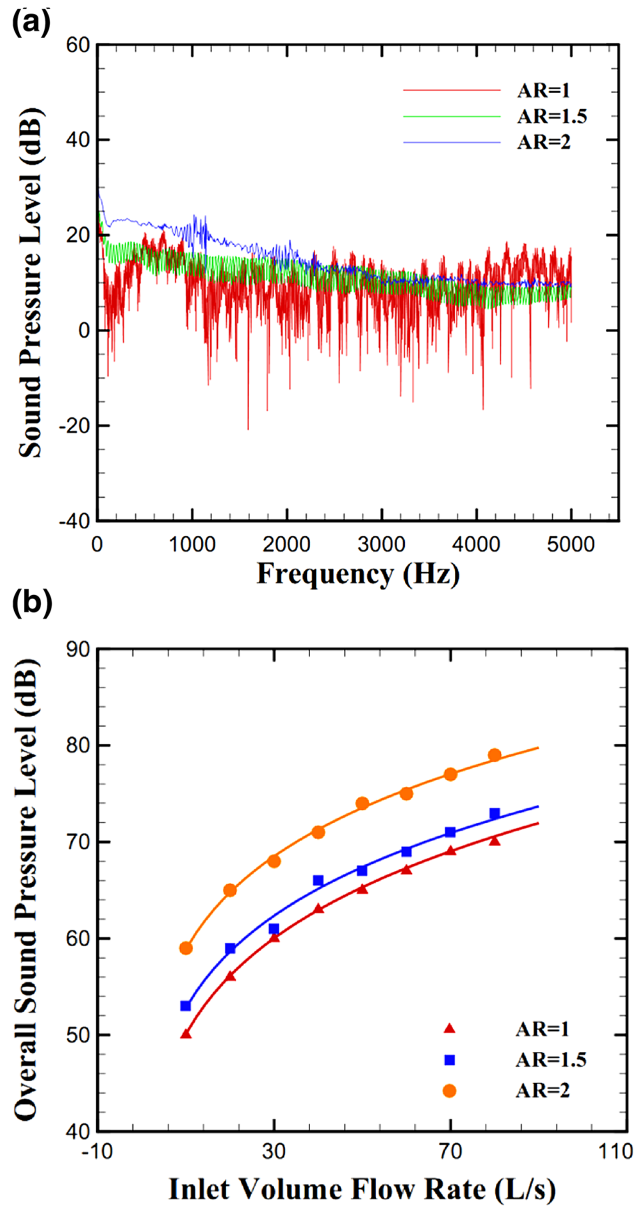

Fig. 14 (a) Sound pressure level of circular Bladeless fan for aspect ratios of 1, 1.5 and 2; (b) Overall sound pressure level of circular fan for aspect ratios of 1, 1.5 and 2

In Fig. 14(b), the OASPL curve for circle fan is shown for aspect ratios of 1, 1.5 and 2. This figure indicates the produced noise is more for high aspect ratios. In addition, the exhausted airflow field from fan is symmetry when the aspect ratio is near 1, but the outlet airflow will not be uniformed and disturbed by increasing of aspect ratio. In Fig. 15(a), the SPL diagram (square fan) with inlet flow rate 30 L/s is depicted for aspect ratios 1, 1.5 and 2. The SPL diagram is indicated in Fig. 15(b) for aspect ratios of 1, 1.5 and 2. As shown in this figure, the generated noise increases by growth of aspect ratio which the reason of this phenomenon mentioned in previous section. In order to compare the acoustic results of circle and square fans, the amount of produced noise by these two fans is compared in Fig. 16. As shown in this figure, the square fan generates much noise with respect to circle one for various inlet flow rate.

9 Conclusions

After studying geometric parameter effects on the aerodynamic performance of a bladeless fan [25–27], in this paper, three-dimensional numerical simulation is investigated to see the effect of geometrical parameters on the

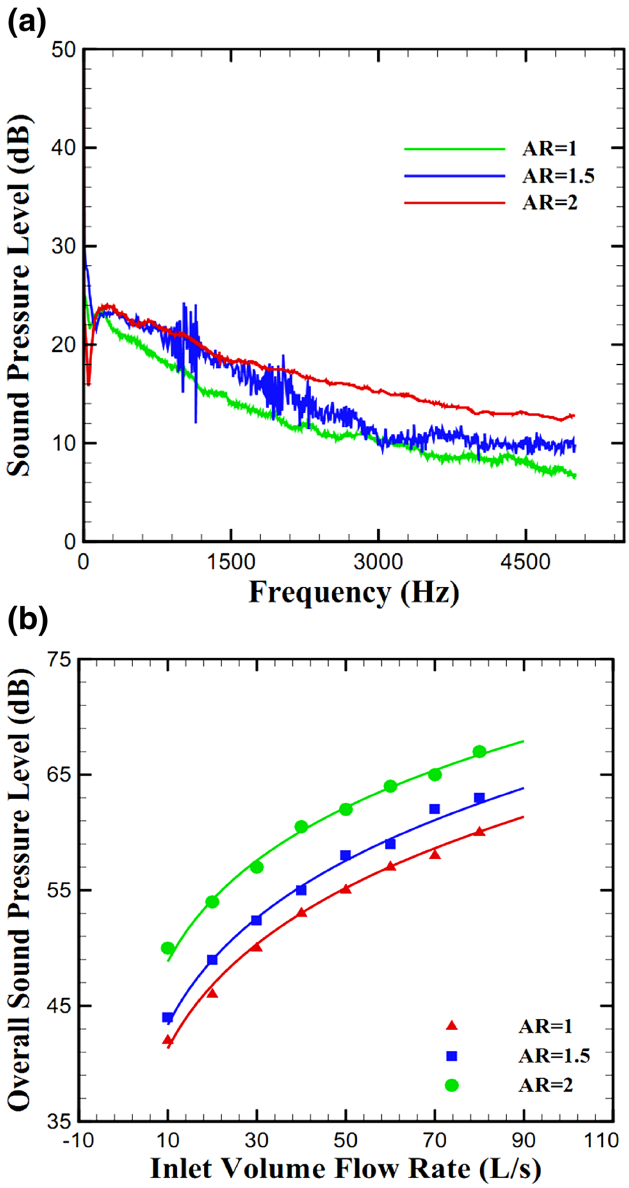

Fig. 15 (a) Sound pressure level of square bladeless fan for aspect ratios of 1, 1.5 and 2; (b) Overall sound pressure level of square fan for aspect ratios of 1, 1.5 and 2

aeroacoustic performances of Bladeless fan. The studied geometric parameters are height of fan cross-section, outlet angle of airflow relative to the fan axis, thickness of outlet slit, hydraulic diameter and aspect ratio. The effect of aspect ratio parameter to assess the effects on the performance of the fan is designed for circle and square shapes. The fan performance have been evaluated by using simulation Bladeless fan inside a cube-shaped room, solving unsteady mass and momentum conservation equations as well as the aeroacoustic equations of FW-H. By comparing the calculated results with experimental data for produced noise of a 2D-airfoil NACA 0012, acoustic code validation

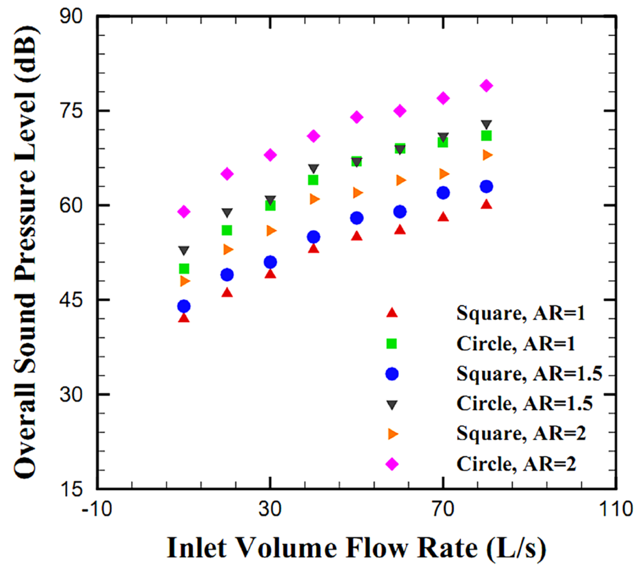

Fig. 16 Comparison of overall sound pressure level of circular and square fan for aspect ratios of 1, 1.5 and 2

is performed. To evaluate the effect of each parameter on the flow increase curve, sound pressure level (SPL) and overall sound pressure level (OASPL) are plotted for different inlet flow rate. The acoustic results show that the generated noise decreases while the height of fan cross section decreases. The obtained results for the outlet angles of 10°, 13°, 16° and 20° show the produced noise increases by increasing the amount of outlet angle. The results for outlet thickness indicate that this parameter is one of the most influential parameters on the aeroacoustic performance of a Bladeless fan. The results for the outlet thicknesses of 1, 2 and 3 mm demonstrate that the produced noise increase significantly by decreasing the outlet thickness. The obtained curves for hydraulic diameters of 30, 60 and 120 cm indicate that the produced noise decreases by increasing the hydraulic diameter of fan. The noise results for this parameter indicate that the generated noise decreases by increasing hydraulic diameter. The aspect ratio of fan is last examined parameter which its effect is investigated on the circle and square Bladeless fan. In addition, the exhausted airflow field from fan is symmetry when the aspect ratio is near 1, but the outlet airflow shall be non-uniform and disturbed by the increasing of aspect ratio. The comparison of acoustic curves between a circle and square fan indicate the aeroacoustic performance of a square fan is a little better than a circle fan. Overall, the results show that the parameters below have the most effective on the aeroacoustic performance of a Bladeless fan respectively. These parameters include outlet thickness, hydraulic diameter, height of fan cross section, aspect ratio, and outlet angle.

References

1. GAMMACK P D, NICOLAS F, SIMMONDS K J. Bladeless fan, in Patent Application Publication. US 2009/0060710Al. United States, 2009.
2. LIN S C, HUANG C L. An integrated experimental and numerical study of forward–curved centrifugal fan. *Experimental Thermal and Fluid Science*, 2002, 26(5): 421-434.
3. CHUNXI L, LING W S, YAKUI J. The Performance of a Centrifugal Fan with Enlarged Impeller. *Energy Conversion and Management*, 2011, 52(8): 2902-2910.
4. GOVARDHAN, M., SAMPAT, D. L. Computational Studies of Flow through Cross Flow Fans-Effect of Blade Geometry. *Journal of Thermal Science*, 2005, 14(3): 220-229.
5. SARRAF C, NOURI H, RAVELET F, et al. Experimental Study of Blade Thickness Effects on the Overall and Local Performances of a Controlled Vortex Designed Axial-Flow Fan. *Experimental Thermal and Fluid Science*, 2011, *35*(4): 684-693.
6. MOHAIDEEN M M. Optimization of Backward Curved Aerofoil Radial Fan Impeller Using Finite Element Modelling. *Procedia Engineering*, 2012, 38: 1592-1598.
7. CHONG T P, JOSEPH P F, KINGAN M J. An Investigation of Airfoil Tonal Noise at Different Reynolds Numbers and Angles of Attack. *Applied Acoustics*, 2012, 74: 38–48.
8. DEVENPORT W J, STAUBS J K, GLEGG S A. Sound Radiation from Real Airfoils in Turbulence. *Journal of Sound and Vibration*, 2010, 329(17): 3470-3483.
9. CASPER J, FARASSAT F. Broadband Trailing Edge Noise Predictions in the Time Domain. *Journal of Sound and Vibration*, 2004, 271(1): 159-176.
10. BALLESTEROS-TAJADURA R, VELARDE-SUAREZ S, HURTADO-CRUZ J. Noise Prediction of a Centrifugal Fan: Numerical Results and Experimental Validation. *J. Fluids Eng.*, 2008, 130(9):091102-091102-12.
11. MOON Y J, CHO Y, NAM H S. Computation of Unsteady Viscous Flow and Aeroacoustic Noise of Cross Flow Fans. *Computers & Fluids*, 2003, 32(7): 995-1015.
12. CHO Y, MOON Y J. Discrete Noise Prediction of Variable Pitch Cross-Flow Fans by Unsteady Navier-Stokes Computations. *ASME Journal of Fluids Engineering*, 2003, *125*(5): 543-550.
13. ENVIA E, WILSON A G, HUFF D L. Fan noise: a challenge to CAA. *International Journal of Computational Fluid Dynamics*, 2004, 18(6): 471-480.
14. YOUNSI M, DJERRADA A, BELAMRI T, et al. Application of the SAS Turbulence Model to Predict the Unsteady Flow Field Behaviour in a Forward Centrifugal Fan. *International Journal of Computational Fluid Dynamics*, 2008, 22(9): 639-648.
15. KHELLADI S, KOUIDRI S, BAKIR F, et al. Predicting Tonal Noise From a High Rotational Speed Centrifugal Fan. *Journal of Sound and Vibration*, 2008, 313(1): 113-133.
16. SORGUVEN E, DOGAN Y, BAYRAKTAR F, et al. Noise prediction via large eddy simulation: Application to radial fans. *Noise Control Engineering Journal*, 2008, *57*(3): 169-178.
17. BROOKS T F, POPE D S, MARCOLINI M A. Airfoil Self-Noise and Prediction. *NASA Reference Publication*. Vol. 1218, 1989.
18. QUINN W R. Upstream Nozzle Shaping Effects on Near Field Flow in Round Turbulent Free Jets. *European Journal of Mechanics-B/Fluids*, 2006, *25*(3): 279-301.
19. DURDIN J. Inventing the 21st Century': An Exhibition at the British Library. *World Patent Information*, 2008, 33(2):190-191.
20. LAUNDER B E, SPALDING D B. Mathematical Models of Turbulence. *Academic Pres*s, 1972, London.
21. WILLIAMS J F, HAWKINGS D L. Sound Generation by Turbulence and Surfaces in Arbitrary Motion. Philosophical Transactions of the Royal Society of London. Series A, *Mathematical and Physical Sciences*, 1969, 264(1151): 321-342.
22. BRENTNER K S, FARASSAT F. Analytical Comparison of the Acoustic Analogy and Kirchhoff Formulation for Moving Surfaces. *AIAA Journal*, 1989, 36(8): 1379-1386.
23. ELENI D C, ATHANASIOS T I, DIONISSIOS M P. Evaluation of the Turbulence Models for the Simulation of the Flow over a National Advisory Committee for Aeronautics (NACA) 0012 Airfoil. *Journal of Mechanical Engineering Research*, 2012, 4(3): 100-111.
24. U.S. National Institute for Occupational Safety and Health (NIOSH), Criteria for a Recommended Standard: Occupational Noise Exposure: Revised Criteria 1998. US Department of Health and Human Services Publication Number,1989, 98-126.
25. JAFARI M, AFSHIN H, FARHANIEH B, et al. Numerical investigation of geometric parameter effects on the aerodynamic performance of a Bladeless fan. *Alexandria Engineering Journal*, 2016, 55(1): 223-233.
26. JAFARI M, AFSHIN H, FARHANIEH B, et al. Numerical aerodynamic evaluation and noise investigation of a bladeless fan. *Journal of Applied Fluid Mechanics*, 2015, 8(1): 133-142.
27. JAFARI M, AFSHIN H, FARHANIEH B, et al. Experimental and numerical investigation of a 60cm diameter bladeless fan. *Journal of Applied Fluid Mechanics*, 2016, 9(2): 935-944.

Mohammad Jafari received B.S. degree from *Isfahan University of Technology, Iran* in 2011, and M.Sc. degree from Mechanical Engineering Department at *Sharif University of Technology* (2013), *Iran*. His research interests are numerical studies in fluid mechanics and heat and mass transfer. He is now a PhD candidate at *Iowa State University, Iowa, United State*. Tel: +1-515-7358099; E-mail: mjafari@iastate.edu

Atta Sojoudi received B.S. degree (with highest honors) from *Tabriz University*, *Iran* in 2012, and M.Sc. degree from Mechanical Engineering Department at *Sharif University of Technology (SUT), Iran*. His research interests are numerical studies in fluid mechanics and heat and mass transfer. He is now a PhD candidate at *University of Tehran, Iran*. Tel: +98-914-1100874; E-mail: meoiotu@yahoo.com

Parinaz Hafezisefat received her B.S. degree from *Isfahan University, Iran* in 2012, and M.Sc. degree from Chemical Engineering Department from *Isfahan University of Technology*, *Iran*, in 2014. Her research interests are numerical and experimental heat transfer. She is now a PhD candidate at *Iowa State University, Iowa, United State*. Tel: +1-515-7356993; E-mail: pa.hfzs@gmail.com